Title
Formation and Stability of C6H3 + Isomers

Journal
The Journal of Physical Chemistry A, 118(43)

ISSN
1089-5639

Authors
Peverati, Roberto
Bera, Partha P
Lee, Timothy J
et al.

Publication Date
2014-10-30

DOI
10.1021/jp5081862

Peer reviewed

On the Formation and Stability of $C_6H_3^+$ Isomers

Journal:	*The Journal of Physical Chemistry*
Manuscript ID:	jp-2014-081862.R1
Manuscript Type:	Article
Date Submitted by the Author:	06-Oct-2014
Complete List of Authors:	Peverati, Roberto; University of California, Berkeley, Chemistry Bera, Partha; NASA Ames Research Center, Code SSA Lee, Timothy; NASA Ames Research Center, Space Science and Astrobiology Division Head-Gordon, Martin; University of California, Berkeley, Chemistry

October 06, 2014

On the Formation and Stability of $C_6H_3^+$ Isomers.

Roberto Peverati,[1,2] Partha P. Bera,[3,4] Timothy J. Lee,[5] and Martin Head-Gordon*[1,2]

[1]*Department of Chemistry, University of California, Berkeley, California, 94720 USA*

[2]*Chemical Sciences Division, Lawrence Berkeley National Laboratory, Berkeley, California, 94720 USA*

[3]*MS 245-6 NASA Ames Research Center, Moffett Field, Mountain View, California, 94035 USA*

[4]*Bay Area Environmental Research Institute, 625 2nd St. Ste 209, Petaluma, CA 94952*

[5]*MS 245-1 NASA Ames Research Center, Moffett Field, Mountain View, California, 94035 USA*

E-mail: mhg@cchem.berkeley.edu

Abstract: The stability of the five main isomers of $C_6H_3^+$ was investigated using quantum chemical calculations. The cyclic isomers are stabilized by two complementary aromatic effects, first 6-electron π aromaticity, and second a more unusual three-center two-electron σ aromaticity. Two cyclic isomers sit at the bottom of the potential energy surface with energies very close to each other, with a third cyclic isomer slightly higher. The reaction barriers for the interconversion of these isomers, as well as to convert to low-energy linear isomers, are found to be very high with transition states that break both the π and the σ aromaticities. Finally, possibilities for forming the cyclic isomers via association reactions are discussed.

***Keywords*:** Astrochemistry, Isomers, Reaction Barriers, Potential Energy Surface, Density Functional Theory.

1. INTRODUCTION

The potential energy surface corresponding to $C_6H_3^+$ stoichiometry is very intriguing from both the computational and the experimental standpoints. The lowest energy isomers on this potential energy surface (PES) belong to two different classes of organic compounds: the cyclic didehydrophenyl cations (**C1**–**C3**) and the protonated hexatriyne chains (**L1**, **L2**), as reported in Figure 1. In terms of chemical bonding, the most interesting isomer on this surface is undoubtedly the 3,5-didehydrophenyl cation (**C1)**: a very stable six-membered cyclic structure that exhibits double aromatic stabilization: a 6-electron π system, and a more unconventional 2-electron, 3-center σ aromatic system. This highly symmetrical D_{3h} symmetry structure was used to introduce the concept of "double aromaticity"—defined as the mutual existence of two delocalized and orthogonal electronic systems in a cyclic molecule—as early as 1979 in the computational work of Chandrashekhar and coworkers.[1] After the interesting concept of double aromaticity was introduced by means of the **C1** isomer, many examples of doubly aromatic compounds have been proposed on the basis of theoretical calculations, and have been confirmed with experiments.[1-15] 3,5-didehydrophenyl cation (**C1)** itself, however, has been proven to be quite elusive to identify experimentally, with only one reported characterization to date.[16] More recent calculations from Schleyer's group,[17] confirmed that the **C1** structure is the global minimum on the $C_6H_3^+$ potential energy surface, while several other theoretical studies from different authors elaborated on the doubly aromatic character by means of molecular orbital analysis and nucleus-independent chemical shift (NICS) calculations.[18,19]

On the experimental side, Nelson and Kenttämaa[16] provided the only experimental evidence of **C1**. The cation was obtained by sustained off-resonance irradiation for collision-

activated dissociation (SORI-CID) of 3,5-dinitrobenzoyl chloride, and identified in a Fourier-transform ion cyclotron resonance spectrometer. The isomers were distinguished by taking advantage of the different reactivity of each isomer with methanol and di-*tert*-butylnitroxide. Their semi-quantitative analysis established that **C1** was present in very small quantities, while the ion population obtained from their dissociative paths was dominated by the linear isomers. To date, no experimental evidence of associative paths that lead to the formation of **C1** has been reported.

A number of experimental studies of acetylene plasmas have produced the $C_6H_3^+$ cation.[20,21] Contreras et al. reported that the intensity of the $C_6H_3^+$ peak in mass spectra in their COSmIC chamber plasma to be the second most intense C6 species after $C_6H_2^+$. Deschenaux et al.[22] observed the formation of $C_6H_3^+$ in their radiofrequency plasmas of acetylene using a mass-spectrum (mass 75). In radiofrequency discharges,[23] acetylene formed various four and six-carbon molecular ions with varying degrees of hydrogenation. While $C_6H_4^+$ represented the largest concentration of six-carbon products, $C_6H_3^+$ was also observed. Ion-molecule reactions of acetylene and its precursors generated in situ can produce more than one isomer of $C_6H_3^+$ in these experiments. $C_6H_3^+$ is also known to form during the photo-destruction of polycyclic aromatic hydrocarbons as shown by Walsh et al.[24] This makes $C_6H_3^+$ a very interesting candidate for detection in the photo-dissociation regions of the circumstellar envelops of carbon rich stars, where PAHs are formed and destroyed by the action of UV-radiation. Although the mass fragment for $C_6H_3^+$ was observed, these experimental studies could not provide any specific insight into which particular isomer or isomers are involved.

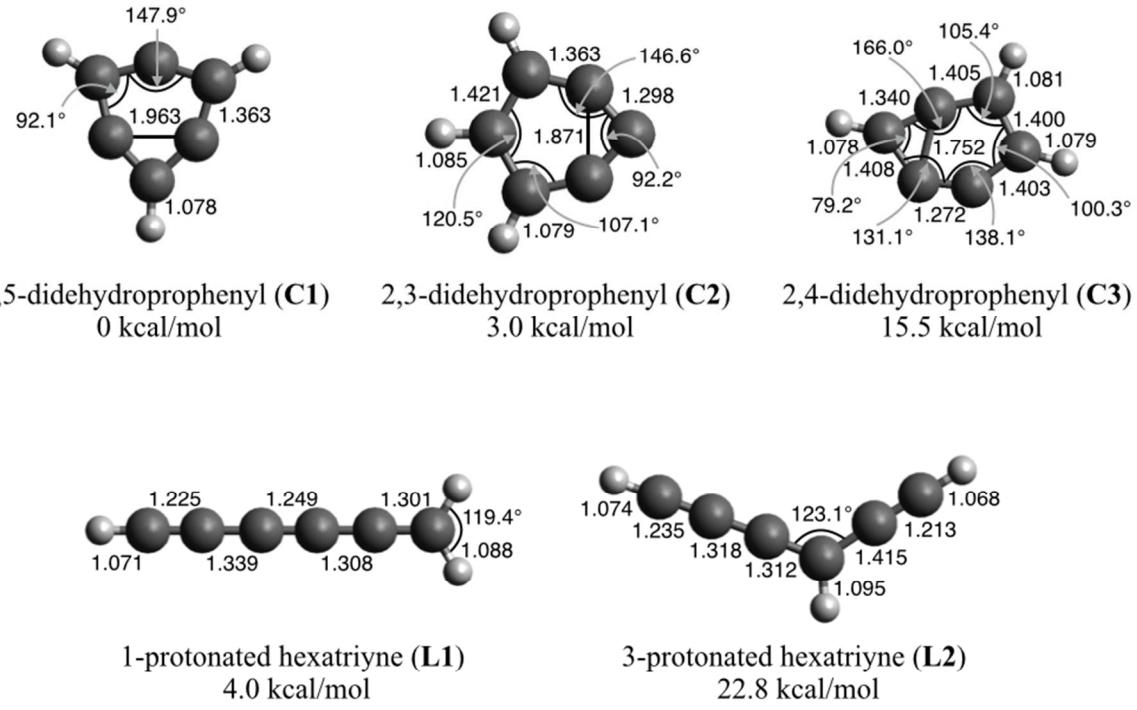

Fig. 1: The lowest energy structures of $C_6H_3^+$. The relative energies (kcal/mol) and geometric parameters (distances in Å, angles in degrees) at the CCSD(T)-F12b/cc-pVTZ+ZPE(B3LYP/cc-pVTZ)//CCSD(T)/cc-pVTZ level are also reported.

In this work, we examine the $C_6H_3^+$ potential energy surface in order to try to shed light on aspects of the potential energy surface, which connect to the experimental challenges associated with preparing and characterizing the low energy isomers. In particular, we put emphasis on the characterization of the transition state structures that connect the five main isomers, and on the topology of the overall potential energy surface. Our results yield some interesting insights into the problem of experimentally preparing the isomers, and also suggest some possible new approaches to isomer preparation. In addition, we consider some aspects of the aromatic electronic structure of the stable cyclic isomers. The remainder of the paper is

laid out as follows. After discussing the electronic structure methods employed in Sec. 2, the structures and relative energies of the low-energy isomers in Fig. 1 are discussed in Sec. 3.1, and the pathways and barriers to interconversion are discussed in Sec. 3.2. In light of these results, and with the aid of *ab initio* trajectory calculations, some possible approaches to isomer isolation are discussed in Sec. 3.3. Conclusions are given in Sec. 4.

2. COMPUTATIONAL METHODS.

Our computational approach is based on the use of all-electron density functional theory (DFT) calculations with different exchange-correlation functionals in conjunction with advanced algorithms for the determination of transition states. The popular B3LYP exchange-correlation functional,[25-27] was used as a primary tool for the initial geometry optimization of the structures because it was found to be suitable for the calculation of geometries and energies of small cationic species.[28] We also validated B3LYP energetic results against more advanced density functional methods, such as M06-2X[29] and ωB97X,[30] as well as wave function methods such as Hartree–Fock (HF) and second order Møller–Plesset perturbation theory (MP2).[31] Finally, our highest quality geometries were optimized using the coupled cluster method with singles, double and perturbative triples (CCSD(T)).[32] All DFT calculations were performed using a very fine integration grid of 99 radial points and 590 angular points. Dunning's correlation consistent valence triple zeta basis set (cc-pVTZ)[33] was used for geometry optimizations and energy analysis. The quality of the results for the minima structures, with particular regards to the convergence of the basis set, were also checked using the CCSD(T)-F12 method (we performed both F12a and F12b methods, and we report the F12b results).[34]

The coupled cluster calculations were performed using the MOLPRO 2008 quantum chemistry code, while all other calculations were performed with the Q-Chem 4.1 quantum chemistry code.[35] For the determination of all the transition states we used the Freezing String Method (FSM)[36,37] followed by transition state search using the Partitioned-Rational Function Optimization (P-RFO) eigenvector-following method.[38] We used hessian calculations to confirm that minima have no imaginary frequencies, and transition states have only one. The reaction path for each transition state was also confirmed by following the intrinsic reaction coordinate along both directions to provide the original reactant and product. In order to avoid the possibility that any obtained structures may have significantly lower energies on the triplet surface, we performed stability analysis on the final wave functions of all the converged structures and transition states using Q-Chem's stability analysis package.

3. RESULTS.

3.1 Stability Of $C_6H_3^+$ Isomers

Results of our calculations on the five considered isomers are reported in Table 1. The CCSD(T)/cc-VTZ values are the highest level results, and the performance of other methods can be assessed relative to them. It is evident the lowest energy structure is **C1** with the **C2** isomer just 2 kcal/mol higher in energy, and the lowest energy chain structure, **L1**, about 5 kcal/mol higher than **C1**. Earlier calculations by Schleyer and coworkers,[17] at the RMP4sdtq/6-31G*//RMP2(fu)/6-31G level, are in qualitative agreement with our CCSD(T) and CCSD(T)-F12 calculations, although the isomers are too far apart in energy. All isomers have been characterized as minima by performing frequency calculations at the B3LYP/cc-pVTZ level. Zero point energy (ZPE) corrections from such calculations have been added to

our electronic energies, and are reported in parentheses in Table 1, while frequencies and IR intensities, as well as Cartesian coordinates for all minima, are reported in the supporting information. The ZPE corrections do not change significantly the picture for the minima, but slightly broaden the differences in energies between **C1, C2,** and **C3**, while reducing the gaps between the cyclic and the linear structures. For example, the stabilization due to ZPE for the linear structure **L1** is about 2.3 kcal/mol larger than that for **C1**, which closes the gap between them.

By comparison, B3LYP erroneously predicts **L1** to be the lowest energy structure, a fact that can be attributed to the well-known erroneous long-range behavior of B3LYP due to long-range self-interaction errors. The long-range character of this error is evidently more pronounced for the linear isomers than for the more compact cyclic isomers. It is interesting to note that while this error strongly affects the relative energies, the B3LYP geometries are very similar to those obtained with CCSD(T). As we report in Table 2, the mean average difference between the B3LYP geometries and the CCSD(T) geometries on all bonds are smaller than 0.01 Å, while the largest difference is smaller than 0.05 Å, confirming that B3LYP is a viable method for the geometry optimization of such systems, while the energies that it provides need to be questioned. The more advanced exchange-correlation methods, M06-2X and ωB97X, provide energetic results that are in much better agreement with each other and with CCSD(T).

Table 1: Energies of $C_6H_3^+$ isomers (in kcal/mol) relative to the global minimum (isomer **C1**), as calculated with different levels of theory (all with the cc-pVTZ basis), and compared to previously published results.[17] B3LYP and CCSD(T) geometries are fully optimized, while all

other methods are single point energies at the B3LYP/cc-pVTZ geometries. In parentheses we report results corrected for zero point energies calculated at the B3LYP/cc-pVTZ level.

	B3LYP	M06-2X	ωB97X	HF	MP2	CCSD(T)	CCSD(T)-F12	Chandrasekhar *et al.*[a]
C1	0.0	0.0	0.0	0.0	0.0	0.0	0.0	0.0
C2	0.9 (2.3)	4.4 (5.8)	0.4 (1.8)	-8.3 (-6.9)	14.5 (15.9)	1.7 (3.1)	1.6 (3.0)	10.7
L1	-10.4 (-12.7)	6.4 (4.1)	4.8 (2.5)	-16.4 (-18.7)	20.4 (18.1)	4.8 (2.4)	6.4 (4.0)	14.1
C3	14.8 (15.5)	16.1 (16.8)	12.7 (13.4)	6.1 (6.8)	24.2 (24.9)	15.1 (15.8)	14.8 (15.5)	23.9
L2	12.6 (10.5)	26.0 (23.9)	22.8 (20.7)	-1.8 (3.9)	40.8 (38.7)	23.5 (21.4)	24.9 (22.8)	33.0

[a]RMP4sdtq/6-31G*//RMP2(fu)/6-31G from ref. [17].

Table 2: Bond lengths (in Å, ordered from the smallest to the largest, see also Fig. 1) of $C_6H_3^+$ isomers: comparison between B3LYP and CCSD(T) results; mean absolute difference (MAD) and largest difference (MaxD).

	C1		C2		C3		L1		L2	
	CCSD(T)	B3LYP	CCSD(T)	B3LYP	CCSD(T)	B3LYP	CCSD(T)	B3LYP	CCSD(T)	B3LYP
1	1.078	1.078	1.079	1.084	1.078	1.077	1.071	1.069	1.068	1.066
2	1.363	1.353	1.085	1.078	1.079	1.078	1.088	1.089	1.074	1.071
3	1.963	1.926	1.298	1.284	1.081	1.080	1.225	1.215	1.095	1.097
4			1.363	1.352	1.270	1.259	1.249	1.241	1.213	1.202
5			1.421	1.415	1.340	1.331	1.301	1.288	1.235	1.225
6			1.871	1.876	1.400	1.397	1.308	1.296	1.312	1.305
7					1.403	1.389	1.339	1.326	1.318	1.305
8					1.405	1.392			1.415	1.400
9					1.408	1.396				
10					1.752	1.751				
MAD		0.016		0.008		0.007		0.008		0.007
MaxD		0.037		0.014		0.014		0.013		0.015

The stability of the cyclic isomers is determined by the interplay of several contributions: i) conventional 6-electron π aromaticity, ii) an unconventional 2-electron σ aromaticity, iii) ring strain effects, and iv) charge delocalization. If we try to distribute the 26 valence electrons we have: 12 electrons in six C-C σ bonds, 6 electrons in three C-H σ bonds,

6 electrons in the π system perpendicular to the molecular plane, for a total of 24 electrons. The remaining two electrons are distributed among the three in-plane orbitals of the three carbon atoms devoid of any hydrogen atoms, with an associated distribution of the net positive charge. The energy differences between **C1**, **C2** and **C3** come from the balance between the two different aromatic stabilizations, the ring strain, and charge delocalization

Changes in the σ system in the 3 isomers manifest themselves in quite striking bond-length and structural differences both relative to each other, and relative to the perfect hexagonal structure of benzene. For the lowest energy isomer, **C1**, which has D_{3h} symmetry, the CC bond length is shortened by 0.04 Å relative to benzene, but the most striking structural change is a 27° CCC bond angle distortion, which leads to short 1.96 Å contacts between the dehydrogenated C atoms. The driving force for this contact is partial bonding character, which is reflected in the σ HOMO, shown in Fig. 2. This orbital can be viewed as the occupied level of a 3-center 2-electron σ aromatic system, consistent with D_{3h} symmetry, which, however, leads to some ring strain.

The **C2** isomer, on the other hand, displays C(H)-C(H) bond lengths that are slightly longer than benzene at 1.42 Å (reflecting some charge delocalization), and a very short 1.30 Å CC bond length, together with a short 1.87 Å CC cross-ring contact. The 1.30 Å CC bond length arises because the 2-electron σ system is concentrated on the CCC side of this isomer, and can be viewed as a σ analog of the π system of the allyl cation. The short cross-ring distance illustrates that there is some remaining σ aromaticity. The lower energy of the **C2** σ HOMO vs. the **C1** σ HOMO reflects symmetry-allowed mixing with other σ orbitals, as corroborated by the higher energies of the lower σ orbitals seen in Fig. 2. The striking difference in high-lying energy levels between **C1** and **C2** suggests that they might be

experimentally distinguished by photoelectron spectroscopy. Despite the slightly higher energy of **C2**, the IP of **C2** is predicted to be about 5 kcal/mol higher than that of **C1** (385 kcal/mol for **C2**, while 380 kcal/mol for **C1** at the M06-2X/cc-pVTZ level).

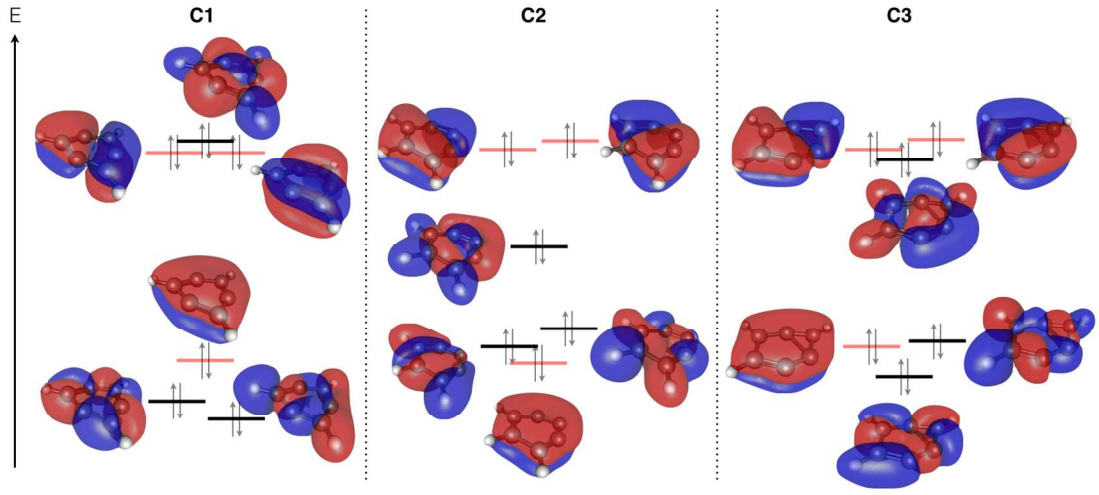

Fig. 2: The six highest occupied molecular orbitals of **C1**, **C2** and **C3** (B3LYP/cc-pVTZ) in $C_6H_3^+$. Orbitals with σ character are indicated with a black line, while orbitals with π character are indicated with a red line.

The third lowest cyclic isomer, **C3**, displays further structural differences relative to **C1** and **C2**. The CC bond length of 1.27 Å is shorter than in **C2**, reflecting some additional localization of the 2-electron σ system, though an even shorter cross-ring contact distance of 1.75 Å accompanies this. This structure is less stable because both the σ and the π systems are distorted, resulting in aromatic stabilization energies that are smaller than for the 2 other cyclic isomers.

In the neutral C_6H_3 radical, tridehydrobenzene (TDB), the extra electron precludes σ aromaticity and results in a completely reversed picture. As already noted in previous studies,[18,39] the ground state of TDB is the 1,2,3-TDB isomer (i.e. C2-like), and it has three unpaired electrons distributed among three nearly degenerate non-bonding σ orbitals. These orbitals resemble the electronic structure of allyl and provide extra stabilization over the other two isomers. 1,3,5-TDB (i.e. C1-like) is the highest energy cyclic isomer on the neutral potential energy surface and since the three σ-orbitals are degenerate, it shows Jahn-Teller distortion from the D_{3h} structure to a lower symmetry C_{2v} structure. In C_6H_3, 1,2,4-TDB has an energy in between 1,2,3-TDB and 1,3,5-TDB. On one side it doesn't have the stabilization due to the 3-center allyl system, but on the other side its orbitals are still non-degenerate and do not cause Jahn-Teller distortion.

An estimation of the stabilization energy in **C1** and **C2** can be achieved by relaxing the internal angles of the 6-membered ring from equal (benzene-like) towards their final optimal values, by constrained optimizations. Figure 3 shows the results of such calculations at the B3LYP/6-311+G* level, with bond lengths either constrained to benzene values, or unconstrained. Figure 3a for **C1** shows that most energy lowering (~55 kcal/mol) is achieved by angle relaxation, rather than by bond relaxation, which accounts for less than 5 kcal/mol. Increasing bond angle alternation brings the three dehydrogenated carbon atoms towards each another, thereby allowing the 3 in-plane σ hybrid orbitals to overlap at the center of the six-membered ring. This provides a three-carbon, two-electron (3C-2e) σ aromatic system in addition to the six-electron π aromatic system. By contrast, as shown in Fig. 3b, for **C2** a large share of relaxation energy is recovered by bond relaxation. When constrained at the bond distances of benzene with only bond angles varied, **C2** recovers about two-thirds of the

relaxation energy. The importance of bond-length changes in **C2** is reflected in the significant bond distance shortening of the CC distances associated with the dehydrogenated carbon atoms already discussed above.

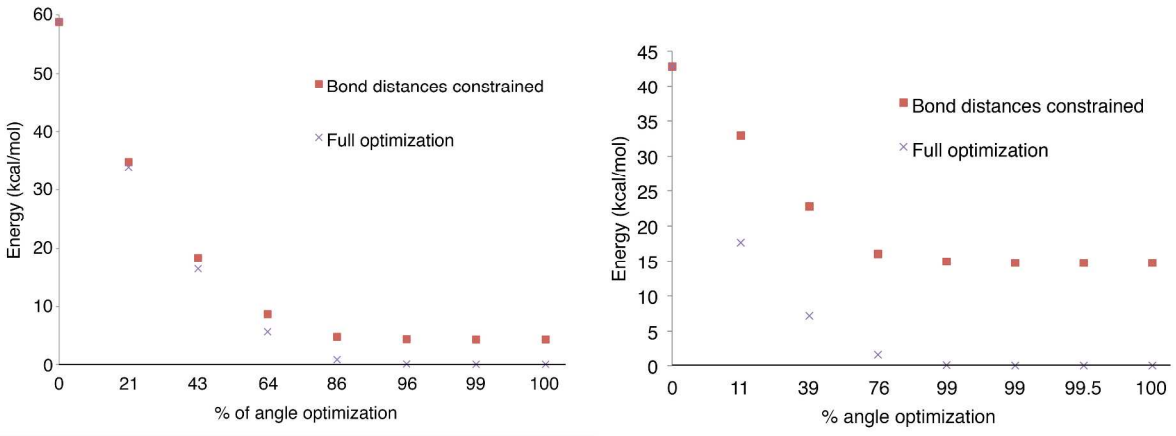

a (**C1**) b (**C2**)

Fig. 3: Bond angle stabilization plot for the two most stable cyclic isomers. The *x*-axis tracks the percentage by which the internal angles of the 6-membered ring are shifted towards their final optimal values (each point represents one step in the optimization). Points labeled with red squares have bond-lengths constrained to their values for benzene, while purple cross points permit full relaxation of bond lengths. It is evident from Fig. 3a that most relaxation energy for **C1** comes from bond angle deformations, whilst bond length relaxation is also important for **C2**.

3.2 Reaction barriers.

We also studied the reaction paths that interconnect the five low-energy isomers belonging to the $C_6H_3^+$ family. The results are summarized in the network diagram shown in Figure 4. On the $C_6H_3^+$ potential energy surface we identified a total of six minimum energy

paths that interconnect the minima, and we optimized the corresponding transition states. Higher energy transition states between minima that are not directly connected might also be possible (e.g., between **C1** and **C2** there is a path that transfers one hydrogen on top of the ring), but the minimum energy paths for these isomerizations very likely go through two transition states (e.g.: **C1** → C1C3 → **C3** → C3C2 → **C2**). The energies of the transition states are reported in Table 3, as calculated with different levels of theory. Stability analysis of all our results confirmed that all closed shell singlet reference determinants were stable, which indicates that there are no lower energy paths possible via spin-crossover.

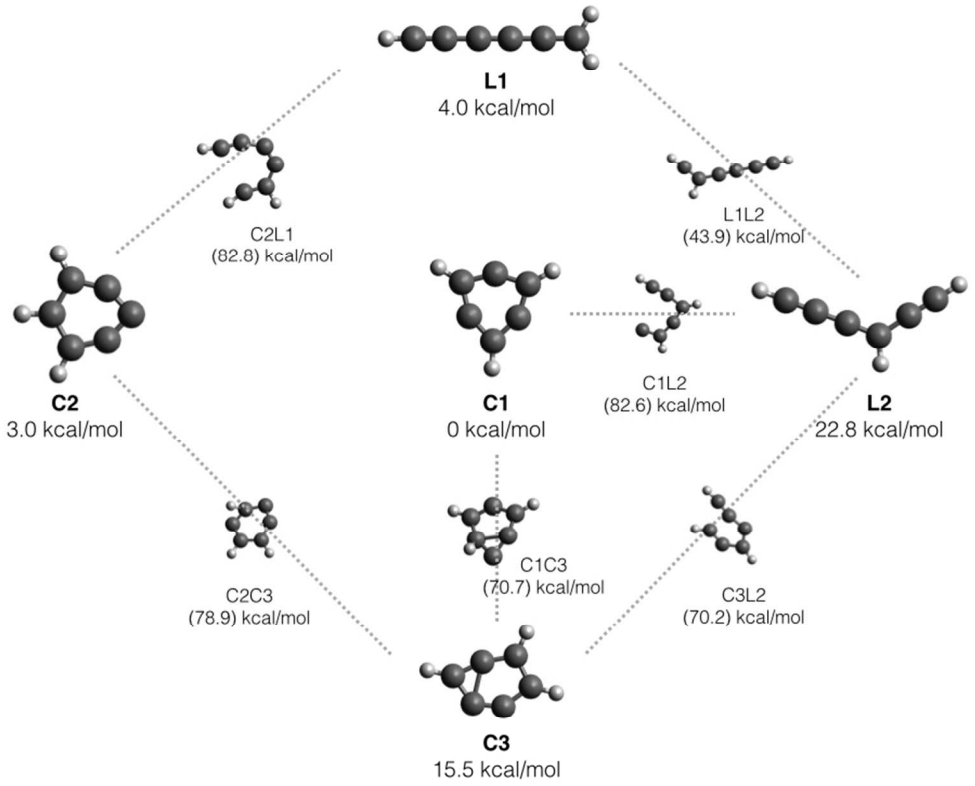

Fig. 4: A two-dimensional network whose vertices are the 5 most stable isomers of $C_6H_3^+$. The edges represent the paths that interconnect them via saddle points that have been located.

The relative energies (CCSD(T)/cc-pVTZ) of the local minima are given in kcal/mol, as well as the energies of the saddle points, also relative to the **C1** global minimum.

Table 3: Barrier heights (kcal/mol) for the interconversion between the three lowest energy isomers of $C_6H_3^+$ (all calculations use B3LYP/cc-pVTZ optimized geometries, and all energies are relative to the lowest energy isomer **C1**. ZPE-corrected results are reported in parentheses.

	B3LYP	M06-2X	ωB97X	CCSD(T)
C1C3	77.3 (73.6)	81.5 (77.8)	82.8 (79.1)	74.4 (70.7)
C1L2	80.3 (76.4)	89.0 (85.1)	86.4 (82.5)	86.5 (82.6)
C2C3	81.5 (78.8)	87.6 (84.9)	84.3 (81.6)	81.6 (78.9)
C2L1	81.1 (77.4)	92.7 (89.0)	90.9 (87.2)	86.5 (82.8)
C3L2	75.8 (73.2)	81.0 (78.4)	81.9 (79.3)	72.8 (70.2)
L1L2	36.7 (32.9)	47.9 (44.1)	45.3 (41.5)	47.7 (43.9)

The most striking feature about the barriers is how high they are, consistent with the closed shell nature of the local minima. The transition state between **C1** and **C3** has a non-planar structure, which involves migration of one hydrogen atom and breaking of the double aromaticity of the isomers. The barrier is 74.4 kcal/mol over **C1** at our best level of theory. An even higher barrier exists for the transition state (C2C3) between **C2** and **C3**, which is 81.6 kcal/mol over the global minimum and breaks both aromaticities. A ring closing takes **L2** to **C3** via a transition state that sits 72.8 kcal/mol above **C1**. Two hydrogen hopping takes **L2** to **L1** via a transition state that is 47.7 kcal/mol above **C1** (the lowest energy barrier located). The transition states between **L1** and **C2** and between **C1** and **L2** involve a hydrogen migration and ring closing/opening. Both these transition states are a very large 86.5 kcal/mol above **C1**.

All the transition states that interconnect the cyclic isomers lie at a very high energy. Zero point vibrational energy (ZPVE) corrections bring these barriers down by roughly 4 kcal/mol, but they remain upwards of 70 kcal/mol. These high barriers are because in addition to the partial breaking of one CH bond before the making of the new one, both the σ and the π aromaticities are broken. For similar reasons the transition states from the linear to the cyclic forms are also at high energies. These high barriers are a strong indication that the experimental identification of one structure over another is due to the path followed to form a given isomer, rather than subsequent isomer interconversion. Interestingly, high-energy transition states are also found for the interconversion between the linear and the cyclic form in neutral C_6H_3.[40] Landera et al. placed the transition state that connects 1,2,3-TDB to 1,2,4-TDB (at the CCSD(T)/CBS//B3LYP/6-311G**+ZPE(B3LYP/6-311G** level) at 68.5 kcal/mol over 1,2,3-TDB,[40] while our best estimation for the cation is C2C3 75.4 kcal/mol over **C2**. The 7 kcal/mol difference is largely because the neutral isomers do not benefit from the double aromatic stabilization.

3.3 Formation pathways to $C_6H_3^+$ isomers.

The presence of very high-energy barriers does not necessarily mean that formation and identification of cyclic $C_6H_3^+$ is impossible under laboratory conditions. Indeed, if cyclic energy minima can be accessed, then because of the high-energy barriers, such species should be identifiable. The question we take up in this section is what formation paths lead to cyclic isomers? The existing results reported by Nelson and Kenttämaa[16] are, to our knowledge, the only experimental indication of the fact that the cyclic $C_6H_3^+$ isomers are stable and can be obtained given appropriately synthesized precursors. However, from a semi-quantitative

analysis of their results, the authors noted that the observed ion population in their experiment "consists mainly of acyclic isomers".[16]

We have performed numerical experiments using *ab initio* molecular dynamics (AIMD) calculations to explore the possibility of forming the **C1** isomer via ion molecule association reactions, starting with the following reaction:

$$C_4H_3^+ + C_2 \rightarrow C_6H_3^+. \qquad \text{(R1)}$$

We chose different initial conditions, with the $C_4H_3^+$ fragment in its global minimum linear geometry, as well as in a higher energy cyclic isomer. The initial relative orientations of the fragments were randomly chosen, and a very small amount of thermal energy (50 K) was provided to initiate the motion of the atoms. The calculations were performed with time steps of 1.21 fs (50 *a.u.*) and for simulation times of 1.2 ps (1000 time steps), using the M06-2X exchange-correlation functional with the cc-pVTZ basis set.

The results of our AIMD calculations show that the formation of the product isomer is strongly related to the structure of the first encounter complex (FEC) for each trajectory. In particular, once we excluded the unreactive scattering paths, we visually inspected the structure of each FEC and found that the majority of the calculations that started from the linear isomer of $C_4H_3^+$ has a FEC that is either linear or branched (e.g. the C_2 fragment attaches with one bond to one C site), and end up in the linear isomer **L1** of $C_6H_3^+$ (90% of the reactive paths). However, the calculations that started from the cyclic isomers of $C_4H_3^+$ have more compact FECs (e.g. the C_2 fragment attaches with more than one bonds and works as a bridge between two or more C sites), and a significantly higher percentage of the simulations ended in one of the stable cyclic minima of $C_6H_3^+$ (37% of the reactive paths). These results are summarized in Figure 5, and reinforce some of our previous findings[41] that in order to

grow cyclic carbon compounds the process of cyclization needs to start early, involving species containing between two and four carbons.

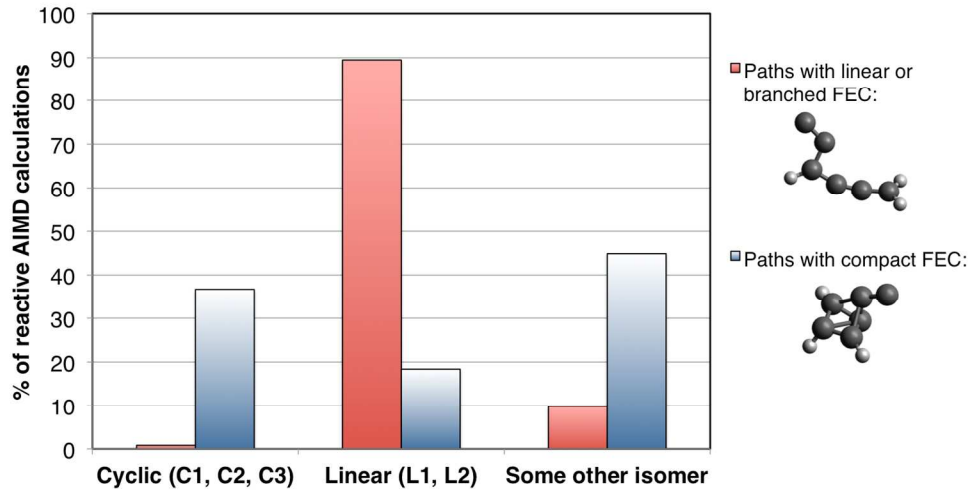

Fig. 5: The fraction of reactive M06-2X/cc-pVTZ AIMD trajectories (111 reactive trajectories out of a total of 200, all with simulation time of 1.2 ps), which finish in linear versus cyclic isomers. The results are binned separately for trajectories that yield a compact first encounter complex (FEC), versus a linear or branched FEC, to show that the product distribution is strongly dependent on this difference.

Reaction R1 could possibly be performed as a molecular beam experiment, or may occur in low-density conditions such as an astrophysical environment. Aspects of the latter conditions have been mimicked in laboratory experiments such as the COSmIC apparatus of Contreras and Salama.[21] If cyclic $C_6H_3^+$ were generated under astrophysical conditions, they could be a precursor to the interstellar formation of larger aromatic compounds, such as polycyclic aromatic hydrocarbons, PAHs.[42] While there are obviously many more association

pathways that may potentially lead to the formation of $C_6H_3^+$ isomers, the previous conclusion that the final product will be related to the shape of the FEC is likely to be transferable.

Dissipating the internal energy of a vibrationally hot product under very low-density conditions is possible by unimolecular dissociation of the hot complex. Therefore $C_6H_3^+$ can also form via the association of smaller species to make a highly energetic $C_6H_4^+$ complex (e.g. by the reaction of acetylene with $C_4H_2^+$) with the consequent elimination of a hot hydrogen atom:[20,23]

$$C_4H_2^+ + C_2H_2 \rightleftarrows [C_6H_4^+]^* \rightarrow C_6H_3^+ + H. \qquad \text{(R2)}$$

The global minimum for $C_6H_4^+$ is more stable than the products of R2 by about 65 kcal/mol (MP2/cc-pVTZ), however the association of acetylene with $C_4H_2^+$ can form an internally 'hot' complex, $[C_6H_4^+]^*$, that can cool by either dissipating energy through collisional transfer of energy, vibrational relaxation or radiative processes, or form $C_6H_3^+$ by expelling a hydrogen atom, as depicted in the diagram of Figure 6.

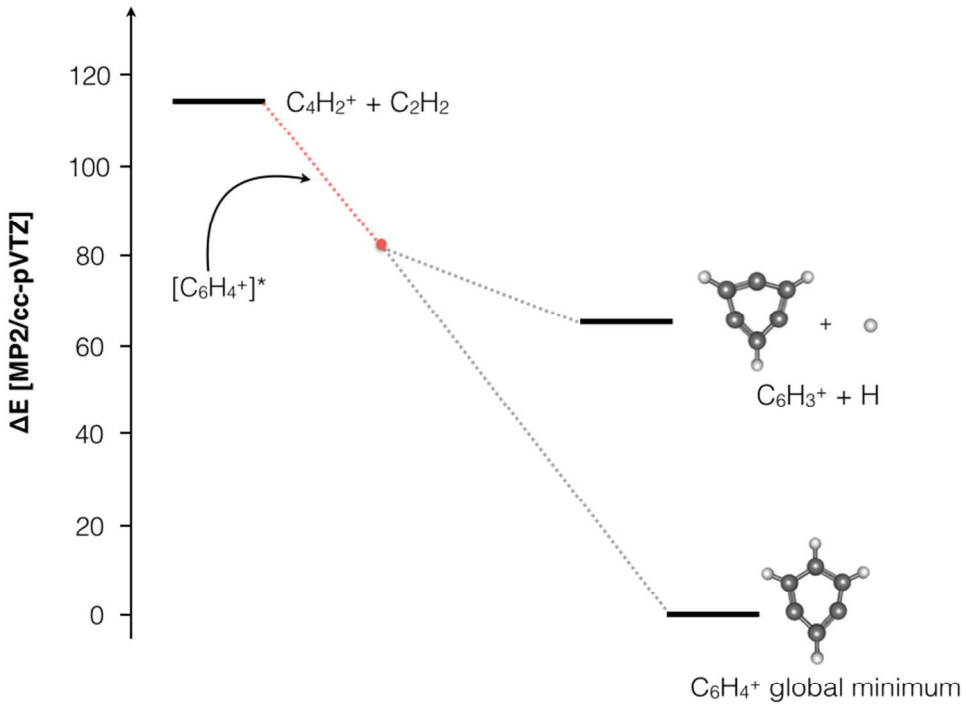

Fig. 6: Possible reaction paths for the association of acetylene with $C_4H_2^+$ (R2).

Finally we should mention that another possible path to forming isomers of $C_6H_3^+$ is via the photoionization of the corresponding neutral radical, C_6H_3. The relative energies of the cyclic conformers of the neutral radical were already discussed in Sec. 3.1. The global minimum of C_6H_3 is the C2-type structure, 1,2,3-TDB. If this conformer were accessed via e.g. collisional stabilization, then subsequent photoionization would access $C_6H_3^+$ in the **C2** structure. However, the question of accessing the global minimum on the neutral C_6H_3 surface via neutral-neutral association reactions is as tricky as accessing particular conformations of the cation: Landera et al note that the $C_4H+C_2H_2$ reaction is predicted to readily produce triacetylene and a hot hydrogen atom.[40]

4. Conclusions.

In this work we report the results on the energetic stability of the main isomers of 3,5-didehydrophenyl cation as well as the barrier heights of reactions between them. In particular, we analyzed five isomers: three with a cyclic structure and two with a linear structure. We revisited the role of aromaticity in stabilizing the cyclic isomers. For transition states, our results show high barriers to interconversion between each cyclic isomer, as well as high barriers for the ring closure reactions that connect the linear isomers to the cyclic ones. This fact might help to shed light on why the cyclic forms of $C_6H_3^+$ are so elusive in experiments with only one identification of such form available to date. In their seminal experimental study, Nelson and coworkers were able to identify small quantities of 3,5-didehydrophenyl cation by using different fragmentation paths in an electron ionization mass spectrometer, but concluded that: "contrary to simple intuition, the formation of the 3,5-didehydrophenyl cation is the exception rather than the rule".[16]

Based on the electronic structure and topology of the potential surface, as well as *ab initio* molecular dynamic simulations, we proposed three different pathways to access the cyclic isomers of $C_6H_3^+$: 1) the association reactions between small fragments such as $C_4H_3^+$ and C_2, 2) the association of $C_4H_2^+$ and C_2H_2 to form a high energy complex, followed by the expulsion of a hot hydrogen atom, and 3) the ionization of the neutral species 1,2,3-tridehydrobenzene, we suggest that these pathways might be accessible under astrophysical conditions, and might be observed in experiments that are conceived to simulate such conditions. The stability of the cyclic forms of $C_6H_3^+$ in these conditions might also be relevant to the genesis of larger aromatic species, such as PAHs.

5. Acknowledgements.

We acknowledge financial support from the NASA *Carbon in the Galaxy* consortium grant NNH10ZDA001N. PPB also acknowledges support from the BAER Institute.

Author Information

Corresponding Author

Martin Head-Gordon (mhg@cchem.berkeley.edu)

Author Contributions

RP and PPB performed the quantum chemistry computations. All authors analyzed the data and wrote the manuscript.

Notes

The authors declare no competing financial interests.

Supporting Information

Infrared frequencies, intensities, and Cartesian coordinates for the minima and transition states on the $C_6H_3^+$ potential energy surface. This material is available free of charge via the Internet at http://pubs.acs.org

6. References.

(1) Chandrasekhar, J.; Jemmis, E. D.; Schleyer, P. v. R. Double Aromaticity: Aromaticity in Orthogonal Planes. the 3, 5-Dehydrophenyl Cation. *Tetrahedron letters* **1979**, *20*, 3707–3710.

(2) Martín-Santamaría, S.; Rzepa, H. S. Double Aromaticity and Anti-Aromaticity in

Small Carbon Rings. *Chem. Commun.* **2000**, 1503–1504.

(3) Zhan, C.-G.; Zheng, F.; Dixon, D. A. Electron Affinities of Aln Clusters and Multiple-Fold Aromaticity of the Square Al4(2-) Structure. *J. Am. Chem. Soc.* **2002**, *124*, 14795–14803.

(4) Präsang, C.; Mlodzianowska, A.; Geiseler, G.; Massa, W.; Hofmann, M.; Berndt, A. Two-Electron Aromatics Containing Three and Four Adjacent Boron Atoms. *Pure Appl Chem* **2003**, *75*, 1175–1182.

(5) Zhai, H.-J.; Kuznetsov, A. E.; Boldyrev, A. I.; Wang, L.-S. Multiple Aromaticity and Antiaromaticity in Silicon Clusters. *Chem. Eur. J. of Chem. Phys.* **2004**, *5*, 1885–1891.

(6) Li, Z.-H.; Moran, D.; Fan, K.-N.; Schleyer, P. v. R. Sigma-Aromaticity and Sigma-Antiaromaticity in Saturated Inorganic Rings. *J. Phys. Chem. A* **2004**, *109*, 3711–3716.

(7) Huang, X.; Zhai, H.-J.; Kiran, B.; Wang, L.-S. Observation of D-Orbital Aromaticity. *Angew Chem Int Edit* **2005**, *44*, 7251–7254.

(8) Tahara, K.; Tobe, Y. Molecular Loops and Belts. *Chem Rev* **2006**, *106*, 5274–5290.

(9) Tsipis, A. C.; Depastas, I. G.; Karagiannis, E. E.; Tsipis, C. A. Diagnosis of Magnetoresponsive Aromatic and Antiaromatic Zones in Three-Membered Rings of D- and F-Block Elements. *J. Comput. Chem.* **2009**, *31*, 431.

(10) Rincon, L.; Almeida, R.; Alvarellos, J. E.; García-Aldea, D.; Hasmy, A.; Gonzalez, C. The Σ Delocalization in Planar Boron Clusters. *Dalton Trans.* **2009**, 3328.

(11) Fowler, P. W.; Mizoguchi, N.; Bean, D. E.; Havenith, R. W. A. Double Aromaticity and Ring Currents in All-Carbon Rings. *Chem-Eur J* **2009**, *15*, 6964–6972.

(12) Jiménez-Halla, J. O. C.; Matito, E.; Blancafort, L.; Robles, J.; Solà, M. Tuning Aromaticity in Trigonal Alkaline Earth Metal Clusters and Their Alkali Metal Salts. *J. Comput. Chem.* **2009**, *30*, 2764–2776.

(13) Liu, C.; Han, P.; Tang, M. Density Functional Theory Study of BnC Clusters. *Rapid Commun. Mass Spectrom.* **2011**, *25*, 1315–1322.

(14) Gilmore, K.; Manoharan, M.; Wu, J. I.-C.; Schleyer, P. v. R.; Alabugin, I. V. Aromatic Transition States in Nonpericyclic Reactions: Anionic 5-Endo Cyclizations Are Aborted Sigmatropic Shifts. *J. Am. Chem. Soc.* **2012**, *134*, 10584–10594.

(15) Wang, C.; Cui, W.; Shao, J.; Zhu, X.; Lu, X. Exploration on the Structure, Stability, and Isomerization of Planar C nB 5(N= 1−7) Clusters. *Int. J. Quantum Chem.* **2013**, *113*, 2514–2522.

(16) Nelson, E. D.; Kenttämaa, H. I. A Fourier-Transform Ion Cyclotron Resonance Study of the 3, 5-Didehydrophenyl Cation. *Journal of the American Society for Mass Spectrometry* **2001**, *12*, 258–267.

(17) Schleyer, P. v. R.; Jiao, H.; Glukhovtsev, M. N.; Chandrasekhar, J.; Kraka, E. Double Aromaticity in the 3, 5-Dehydrophenyl Cation and in Cyclo [6] Carbon. *J. Am. Chem. Soc.* **1994**, *116*, 10129–10134.

(18) Nguyen, H. M. T.; Höltzl, T.; Gopakumar, G.; Veszpremi, T.; Peeters, J.; Nguyen, M. T. Energetics and Chemical Bonding of the 1,3,5-Tridehydrobenzene Triradical and Its Protonated Form. *Chem. Phys.* **2005**, *316*, 125–140.

(19) Wodrich, M. D.; Corminboeuf, C.; Park, S. S.; Schleyer, P. v. R. Double Aromaticity in Monocyclic Carbon, Boron, and Borocarbon Rings Based on Magnetic Criteria. *Chem-Eur J* **2007**, *13*, 4582–4593.

(20) Benedikt, J. Plasma-Chemical Reactions: Low Pressure Acetylene Plasmas. *J. Phys. D: Appl. Phys.* **2010**, *43*, 043001.

(21) Contreras, C. S.; Salama, F. Laboratory Investigations of Polycyclic Aromatic Hydrocarbon Formation and Destruction in the Circumstellar Outflows of Carbon Stars. *ApJS* **2013**, *208*, 6.

(22) Deschenaux, C.; Affolter, A.; Magni, D.; Hollenstein, C.; Fayet, P. Investigations of CH4, C2H2 and C2H4 Dusty RF Plasmas by Means of FTIR Absorption Spectroscopy and Mass Spectrometry. *J. Phys. D: Appl. Phys.* **1999**, *32*, 1876.

(23) Vasile, M. J.; Smolinsky, G. The Chemistry of Radiofrequency Discharges: Acetylene and Mixtures of Acetylene with Helium, Argon and Xenon. *Int. J. Mass Spectrom. & Ion Phys.* **1977**, *24*, 11–23.

(24) Walsh, A. J.; Ruth, A. A.; Gash, E. W.; Mansfield, M. W. D. Multi-Photon UV Photolysis of Gaseous Polycyclic Aromatic Hydrocarbons: Extinction Spectra and Dynamics. *J. Chem. Phys.* **2013**, *139*, 054304.

(25) Becke, A. D. Density-Functional Exchange-Energy Approximation with Correct Asymptotic-Behavior. *Phys. Rev. A* **1988**, *38*, 3098–3100.

(26) Becke, A. D. Density-Functional Thermochemistry. 3. the Role of Exact Exchange. *J. Chem. Phys.* **1993**, *98*, 5648–5652.

(27) Stephens, P.; Devlin, F.; Chabalowski, C.; Frisch, M. J. Ab-Initio Calculation of Vibrational Absorption and Circular-Dichroism Spectra Using Density-Functional Force-Fields. *J. Phys. Chem.* **1994**, *98*, 11623–11627.

(28) Bera, P. P.; Head-Gordon, M.; Lee, T. J. Association Mechanisms of Unsaturated C2 Hydrocarbons with Their Cations: Acetylene and Ethylene. *Phys. Chem. Chem. Phys.* **2013**, *15*, 2012–2023.

(29) Zhao, Y.; Truhlar, D. G. The M06 Suite of Density Functionals for Main Group Thermochemistry, Thermochemical Kinetics, Noncovalent Interactions, Excited States, and Transition Elements: Two New Functionals and Systematic Testing of Four M06-Class Functionals and 12 Other Functionals. *Theor. Chem. Acc.* **2008**, *120*, 215–241.

(30) Chai, J.-D.; Head-Gordon, M. Systematic Optimization of Long-Range Corrected Hybrid Density Functionals. *J. Chem. Phys.* **2008**, *128*, 084106.

(31) Moller, C.; Plesset, M. Note on an Approximation Treatment for Many-Electron Systems. *Phys. Rev.* **1933**, *46*, 0618–0622.

(32) Raghavachari, K.; Trucks, G. W.; Pople, J. A.; Head-Gordon, M. A 5th-Order Perturbation Comparison of Electron Correlation Theories. *Chem. Phys. Lett.* **1989**, *157*, 479–483.

(33) Kendall, R. A.; Dunning, T. H.; Harrison, R. Electron-Affinities of the 1st-Row Atoms Revisited - Systematic Basis-Sets and Wave-Functions. *J. Chem. Phys.* **1992**, *96*, 6796–6806.

(34) Adler, T. B.; Knizia, G.; Werner, H.-J. A Simple and Efficient CCSD(T)-F12 Approximation. *J. Chem. Phys.* **2007**, *127*, 221106.

(35) Shao, Y.; Gan, Z.; Epifanovsky, E.; Gilbert, A. T. B.; Wormit, M.; Kussmann, J.; Lange, A. W.; Behn, A.; Deng, J.; Feng, X.; et al. Advances in Molecular Quantum Chemistry Contained in the Q-Chem 4 Program Package. *Mol. Phys.* **2014**, *in press*, DOI:10.1080/00268976.2014.952696.

(36) Behn, A.; Zimmerman, P. M.; Bell, A. T.; Head-Gordon, M. Efficient Exploration of

Reaction Paths via a Freezing String Method. *J. Chem. Phys.* **2011**, *135*, 224108.

(37) Mallikarjun Sharada, S.; Zimmerman, P. M.; Bell, A. T.; Head-Gordon, M. Automated Transition State Searches Without Evaluating the Hessian. *J. Chem. Theory Comput.* **2012**, *8*, 5166–5174.

(38) Baker, J. An Algorithm for the Location of Transition States. *J. Comput. Chem.* **1986**, *7*, 385–395.

(39) Bettinger, H. F.; Schleyer, P. v. R.; Schaefer, H. F., III. Tetradehydrobenzenes: Singlet−Triplet Energy Separations and Vibrational Frequencies. *J. Am. Chem. Soc.* **1999**, *121*, 2829–2835.

(40) Landera, A.; Krishtal, S. P.; Kislov, V. V.; Mebel, A. M.; Kaiser, R. I. Theoretical Study of the C6H3 Potential Energy Surface and Rate Constants and Product Branching Ratios of the C2H(2Σ+)+C4H2(1Σg+) and C4H(2Σ+)+C2H2(1Σg+) Reactions. *J. Chem. Phys.* **2008**, *128*, 214301.

(41) Bera, P. P.; Head-Gordon, M.; Lee, T. J. Initiating Molecular Growth in the Interstellar Medium via Dimeric Complexes of Observed Ions and Molecules. *Astronomy and astrophysics* **2011**, *535*, A74.

(42) Lovas, F.; McMahon, R.; Grabow, J. U.; Schnell, M.; Mack, J.; Scott, L. T.; Kuczkowski, R. Interstellar Chemistry: a Strategy for Detecting Polycyclic Aromatic Hydrocarbons in Space. *J. Am. Chem. Soc.* **2004**, *127*, 4345–4349.

TOC Graphic